ELSEVIER

Polymer 41 (2000) 7793–7802

polymer

Orientation prior to crystallisation during drawing of poly(ethylene terephthalate)

D.J. Blundell[a,b], A. Mahendrasingam[a,*], C. Martin[a], W. Fuller[a], D.H. MacKerron[c], J.L. Harvie[c], R.J. Oldman[b], C. Riekel[d]

[a]*Department of Physics, Keele University, Staffordshire ST5 5BG, UK*
[b]*ICI Technology, P.O. Box 90, Wilton, Middlesbrough, Cleveland TS90 8JE, UK*
[c]*DuPont UK Ltd, P.O. Box 2002, Wilton, Middlesbrough, Cleveland TS90 8JF, UK*
[d]*ESRF, BP 220, F-38043 Grenoble Cedex, France*

Received 26 July 1999; received in revised form 16 December 1999; accepted 14 February 2000

Abstract

Wide angle X-ray scattering data have been recorded during the drawing of poly(ethylene terephthalate) (PET) using a wide range of draw rates (0.05–12 s^{-1}), temperatures (90–120°C) and draw ratios. The data were analysed to follow the development of molecular orientation and the onset of crystallisation. The molecular orientation prior to crystallisation has been characterised in terms of the orientation order parameter $\langle P_2(\cos\theta)\rangle$. The rate of increase of $\langle P_2(\cos\theta)\rangle$ with draw ratio decreases with both increasing temperature and decreasing draw rate. A superposition of all the data to a common reference temperature of 90°C was obtained using a WLF shift factor to provide a master curve showing the dependence of the development of $\langle P_2(\cos\theta)\rangle$ on draw rate. A comparison of the known chain relaxation motions of PET with the observed relation between draw rate and the onset of crystallisation provides an explanation of a previous discrepancy in the literature concerning the point of onset of crystallisation. For draw rates faster than the rate of the chain retraction motion, the onset of crystallisation is delayed until the end of the deformation process. For draw rates slower than the chain retraction motion, there is evidence of the onset of crystallisation occurring before the end of the deformation process.

Keywords: Poly(ethylene terephthalate); Orientation; Crystallisation

1. Introduction

Poly(ethylene terephthalate) (PET) is used extensively in the manufacture of fibres, bottles and films. All of these applications make use of PET in the oriented crystalline state. Although there is an extensive literature on the crystallisation of PET from the unoriented state, there has been relatively little information on the faster crystallisation process that occurs in an oriented polymer. However recent studies using synchrotron radiation have for the first time enabled real-time observation of oriented crystallisation during drawing at fast rates comparable to industrial processing conditions [1,2]. These experiments revealed behaviour which differed from that deduced from laboratory experiments carried out at slower draw rates or those in which samples were quenched to room temperature before characterising the crystallinity [4,5].

In the drawing conditions previously examined (85–110°C at strain rates of $\sim$10 s^{-1}), it was found that irrespective of the final draw ratio the crystallisation process did not commence until after the completion of the extension process [2]. This contrasted with previous expectations that crystallisation starts at a particular stage in the extension process. Some recent real-time experiments of Middleton et al. [6] using both laboratory and synchrotron observations have now provided definitive evidence of crystallisation occurring before the end of draw when drawing at slower rates ($\sim < 0.1$ s^{-1}). This indicates that the onset of crystallisation depends on the drawing rate and that there is a possible change in polymer behaviour when drawing at faster rates.

It was also found in the previous study [2] that the subsequent crystallisation rate was strongly dependent on the final draw ratio but was apparently insensitive to changes in temperature. This surprising lack of temperature dependence was attributed to the participation of local chain

* Corresponding author. Tel.: +44-1782-583312; fax: +44-1782-711093.
E-mail address: a.mahendrasingam@keele.ac.uk (A. Mahendrasingam).

0032-3861/00/$ - see front matter
PII: S0032-3861(00)00128-2

motions that were insensitive to temperature. However there was also a suspicion that there may be two processes involved with opposing temperature dependence.

This previous study also illustrated two of the bounds of the regime in which oriented crystallisation occurs. No oriented crystallisation was observed at temperatures above 125°C. Also while drawing at 90°C, no crystallisation occurred for draw ratios below ~2.0:1. Both these bounds emphasise the importance of achieving a critical degree of segment orientation to enable the rate of the crystallisation process to compete with chain relaxation processes.

In order to clarify these issues, further synchrotron experiments have now been carried out in which the effect of the rate of draw has been examined together with its interrelation with the draw temperature. A method has now been developed for analysing the diffraction data to obtain a quantitative estimate of the molecular orientation in the deforming polymer, thus enabling the temperature-rate equivalence principle to be explored. Some of the main observations have been summarised in a previous note [3]. The present paper reports in detail the results of these new studies in characterising the chain segment orientation that occurs during the extension process prior to the onset of oriented crystallisation. The results are discussed in relation to chain network relaxation processes and in particular to the relaxation time τ_B of chain retraction in a strained, entangled network. It is shown that the build up of segment orientation and the subsequent crystallisation behaviour depends on whether the rate of draw is greater or less than the retraction rate, $1/\tau_B$. This analysis helps explain the discrepancies in the previous literature. A more detailed analysis of the crystallisation rates and of how they depend on molecular orientation and temperature will be presented in a subsequent paper [20].

2. Experimental

The wide angle X-ray diffraction data was recorded on beamline ID13 at the ESRF in Grenoble using an X-ray camera that had been purpose designed and constructed in the Keele Physics Department workshops. It consisted of a $150 \times 150 \times 150$ mm^3 oven made of aluminium plates of which three sides were made to be interchangeable so that it was possible to exchange sides depending on the particular application. This allowed the viewing port in which the video camera was mounted to be varied according to the overall size and shape of the specimen being studied. The oven was heated electrically by elements mounted on the top and bottom of its interior and the temperature was kept uniform by the use of an air circulating fan. The temperature of the oven could be controlled to within 1°C and the maximum temperature available was 350°C. The sample of PET was clamped between two jaws attached to stepper motors, which allowed uniaxial bi-directional drawing at rates up to about 10 s^{-1}. The beamline ID13 used a mirror monochromator to produce a highly collimated beam 30 μm diameter with a wavelength of 0.92 Å. Diffraction patterns were recorded using a Photonics Science CCD detector with a sensitive area 92×69 mm^2 and an effective pixel area of 120×120 μm^2. The specimen-detector distance could be as small as 6 cm. Diffraction patterns were recorded with exposure times of 40 ms. Over this period, the pattern was integrated within the detector before being digitised by a Synoptic i860 framegrabber within an 8-bit word. 124 frames of 512×512 pixels or 496 of 256×256 pixels could be recorded "end-to-end" with essentially no dead-time between frames before the memory of the frame grabber was full, at which point they were downloaded through a SCSI interface to a Pentium PC.

Specimens 10 mm wide were cut from a sheet of 840 μm thick cast film of amorphous unoriented PET with a number average molecular weight of ~20,000. Ink reference stripes were drawn with a separation of 1 mm on the specimen at right angles to the draw direction to enable the degree of extension to be deduced from the video camera image. The specimen was mounted in the jaws of the camera with a 10 mm gauge length. The control of the stepper motors of the camera was set to move the jaws apart at the desired extension rate. Each specimen was heated in the camera to the required draw temperature and allowed to equilibrate for 2 min. They were then drawn to various final draw ratios by stopping the motors after a predefined number of steps.

A systematic series of drawing experiments were carried out to cover a matrix of temperatures (90, 100, 110, 120°C) and nominal draw rates (1.5 and 12 s^{-1}). For most combinations of temperature and draw rate, several final draw ratios were obtained covering the range from the lowest limit where crystallisation failed to occur to an upper limit of around 3.5:1. In addition to these experiments, a larger range of draw rates was examined at 90°C from 0.12 to 12 s^{-1}.

In order to quantify the development of orientation during deformation but before crystallisation, azimuthal circular scans were extracted from the 2D data frames at a reciprocal space vector of ~0.28 Å^{-1}. This corresponds to the position of the maximum in the equatorial scans of the diffuse diffraction observed at the onset of crystallisation. Radial scans were chosen to obtain an estimate for the background level. There is an expectation that this azimuthal profile is closely linked to the orientation distribution of the segments making up the PET chain. This is analogous to the distribution of crystalline chains in crystallised oriented PET being directly linked with the azimuthal profile of {*hk*0} reflections. This link is not strictly rigorous for non-crystalline segments but has been found to give realistic estimates of orientation distributions by other authors [7,8]. It is generally accepted that the strong diffraction halo at around ~0.28 Å^{-1} in amorphous polymers is attributed to interference between scattered radiation from segments of neighbouring chains. This diffraction will be at a maximum when the scattering vector is mutually perpendicular to the direction vectors of neighbouring segments and as such

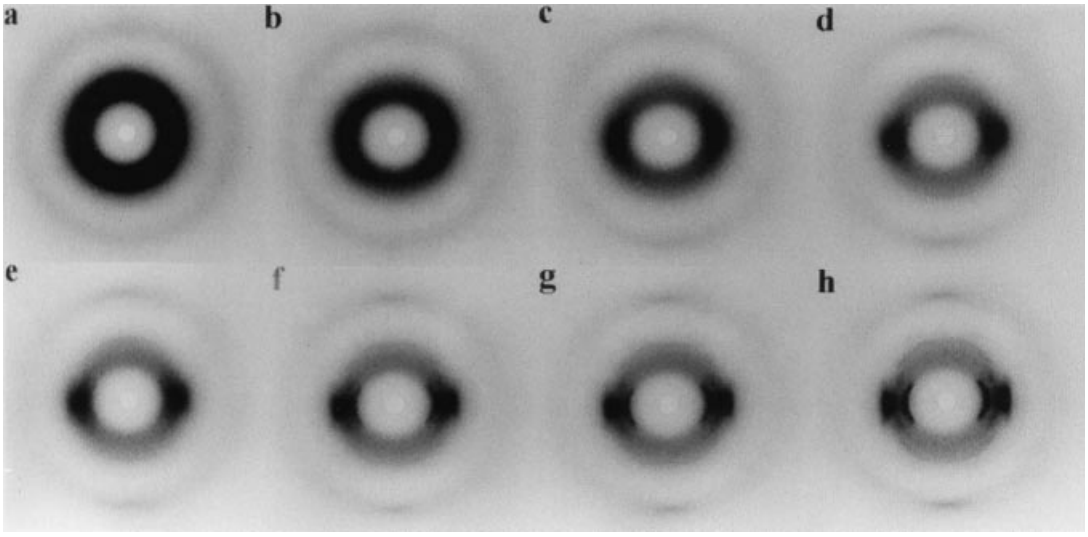

Fig. 1. Selected X-ray diffraction patterns of a PET sample drawn at 90°C and draw rate 3.5 s^{-1}. Diffraction patterns (a)–(c) corresponding to frames 1, 8, 12 and (d)–(h) corresponding to frames 16, 20, 24 and 124. Each frame was recorded in 40 ms with no "dead-time" between frames.

will give an azimuthal profile that follows the distribution of vectors at right angles to the non crystalline segments on the assumption that the structure within the specimen has uniaxial symmetry. The azimuthal profiles were used to calculate the orientation order parameter $\langle P_2(\cos\theta)\rangle$, using the expression derived by Lovell and Mitchell [9], where θ is the angle between the segment direction and the draw direction.

A major issue with constant rate drawing experiments is that the mode of deformation of the polymer can be unpredictable and depends on the drawing conditions. At lower temperatures and faster draw rates, where the yield stress is higher, there is a greater tendency to localised necking so that the local draw ratio and draw rate of the portion being traversed by the X-ray beam is higher than that suggested by the separation of the clamps. Two methods were adopted for monitoring the draw ratio of the sample at the position penetrated by the incident X-ray beam. The first used the video image to measure the separation of markings on the sample. This was supplemented by a method based on the integrated scattered intensity from the sample. The second method has the merit that this is directly linked with the part of the sample from which the X-ray data is recorded. If it is assumed that the sample density remains constant during the draw and that the shape of the sample changes in an affine way, then for a draw ratio of λ, the thickness of the sample in the beam direction would be proportional to $1/\sqrt{\lambda}$. Thus the square of the inverse of the integrated intensity should be directly proportional to λ. In practice the deformation is not ideally uniaxial and in order to obtain absolute values for the draw ratio it is necessary to use a calibrated curve from experiments in which corresponding video image and integrated intensity measurements were made on the same specimens. The intensity method is particularly suited for analysing large data sets and is the preferred way of identifying the points where changes in deformation are occurring and in particular where the local deformation has stopped.

Estimates of crystallinity were obtained from radial scans along the equator by fitting a Pearson VII function to the (010) crystal reflection, using the procedures reported previously [1].

3. Results

A representative set of diffraction frames is shown in Fig. 1 for a draw temperature of 90°C and a nominal draw rate of 3.5 s^{-1}. Fig. 1a–c show the development of the pattern during the deformation process from an unoriented broad halo to an oriented non-crystalline pattern at the end of the draw. Subsequent development of crystalline diffraction is shown in Fig. 1d–h.

Fig. 2 shows plots from the full set of frames recorded in this experiment of the draw ratio derived from the integrated intensity and the crystallinity index derived from equatorial scans. The full line on this plot is a fit to the crystallinity data based on a first order transformation process, using the procedures described in previous papers [1,2]. The predicted start of the crystallisation process from this fit coincides closely with the end of draw derived from the integrated intensity. This confirms our previous conclusion that for fast draw rates the onset of crystallisation does not occur until the end point of the deformation stage.

Fig. 3 shows a similar plot for an experiment carried out at 90°C and a nominal final draw ratio of 3.5:1 for a faster draw rate of 11.5 s^{-1}. Fig. 4 shows corresponding data for a slower draw rate of 0.56 s^{-1}. The compression of events at the faster rate in Fig. 3 makes it more difficult to resolve the crystallisation onset relative to the end of deformation but

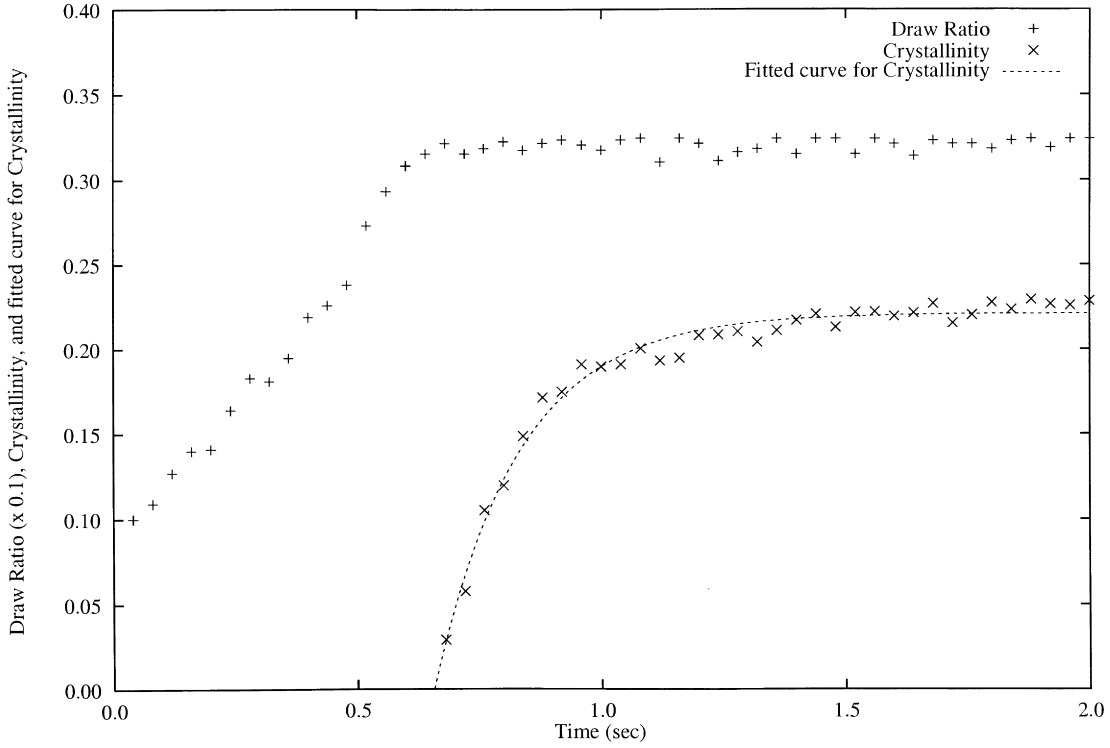

Fig. 2. Plot of the variation in draw ratio (+), crystallinity (×) calculated from the sequence of X-ray diffraction patterns of the PET sample recorded during the drawing at 90°C and draw rate 3.5 s^{-1}. The dotted line indicates the fitted curve based on a first order transformation for the crystallisation process.

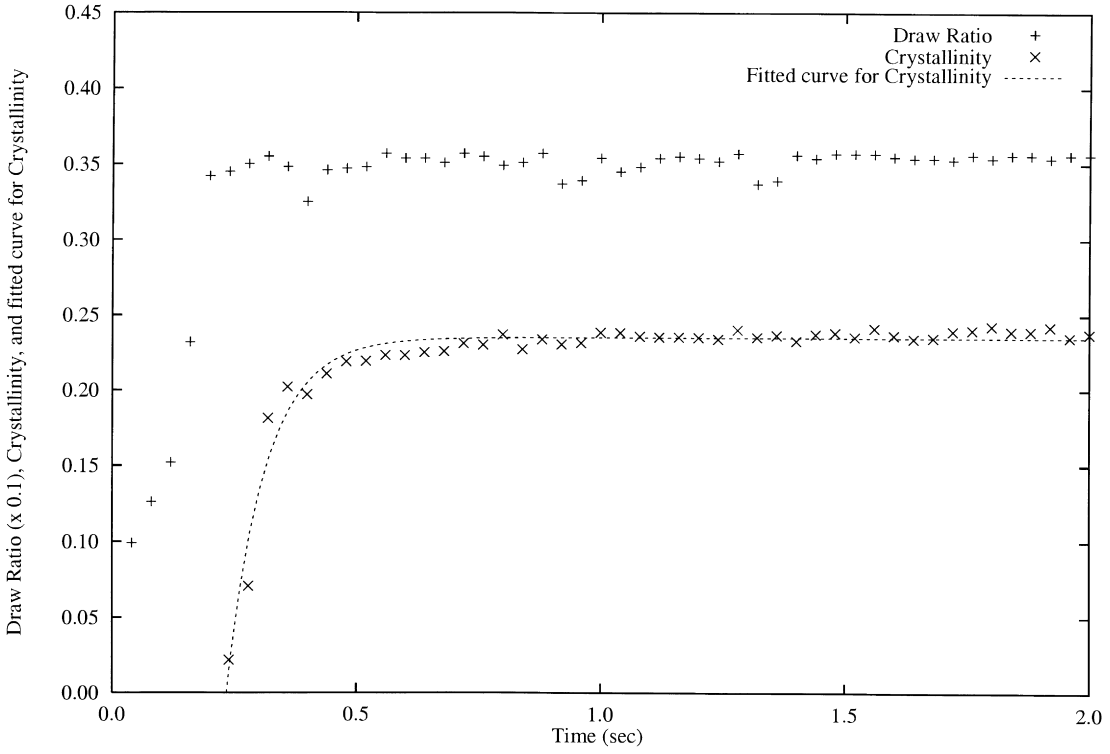

Fig. 3. Plot of the variation in draw ratio (+), crystallinity (×) calculated from the sequence of X-ray diffraction patterns of the PET sample recorded during the drawing at 90°C and draw rate 11.5 s^{-1}. The dotted line indicates the fitted curve based on a first order transformation for the crystallisation process.

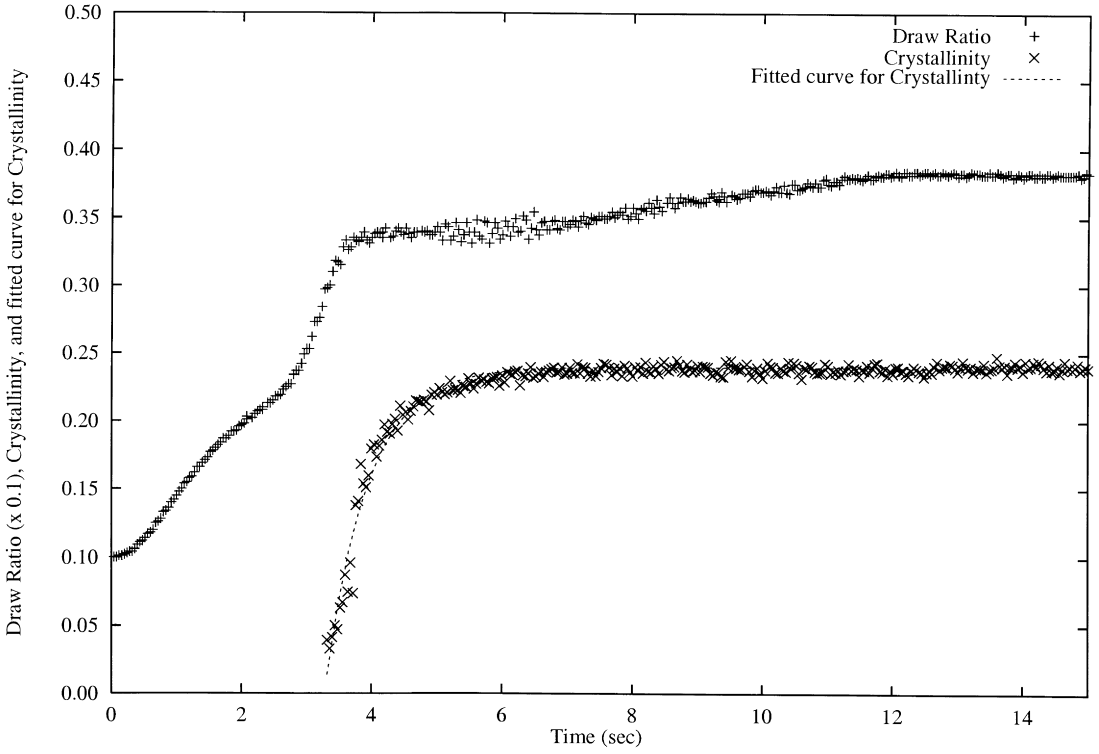

Fig. 4. Plot of the variation in draw ratio (+), crystallinity (×) calculated from the sequence of X-ray diffraction patterns of the PET sample recorded during the drawing at 90°C and draw rate 0.56 s^{-1}. The dotted line indicates the fitted curve based on a first order transformation for the crystallisation process.

within experimental accuracy the data is fully consistent with previous observations. However at the slower draw rate in Fig. 4 there is now clear evidence that the crystallisation process starts before the end of the extensional deformation. Furthermore the crystallisation process appears to be deviating from the simple first order transformation behaviour. The change in slope of the draw ratio data suggests the crystallisation may be interacting with the deformation process.

This change in behaviour at slower draw rates explains the discrepancy with the recent results of Middleton et al. [6] and indicates that there are two regimes of behaviour for the oriented crystallisation process. In order to clarify this observation, the end point of deformation and the onset point of crystallisation were identified for a series of experiments carried out at 90°C covering draw rates from 0.12 to 12.8 s^{-1}. Table 1 lists the frame numbers corresponding to these points and also shows estimates of the crystallinity attained at the end point of drawing as a percentage of final crystallinity achieved at the end of experiment. It will be noted from Table 1 that the draw rate at which crystallisation starts before the end of draw is around 1 s^{-1}. For draw rates faster than this, the onset of the crystallisation process closely coincides with the end of the deformation phase. For slower draw rates there is evidence that crystallisation starts increasingly earlier in the deformation process.

Fig. 5 shows examples of background corrected azimuthal scans obtained from selected frames from the drawing experiment illustrated in Fig. 1. The $\langle P_2(\cos\theta)\rangle$ orientation parameter derived from the azimuthal profiles is shown in Fig. 6 plotted against true draw ratio for all the frames from this experiment up to the end point of the deformation process. Frames beyond the end of deformation contain increasing contributions from crystalline diffraction, which complicate the interpretation of the orientation parameter. Also shown for comparison in Fig. 6 are corresponding plots for other drawing experiments carried out with different

Table 1
Point of onset of crystallisation and extent of crystallisation at the end of draw when drawing at 90°C at different draw rates to a nominal draw ratio of 3.5:1

Draw rate (s^{-1})	End of draw frame number	Start of crystallisation frame number	% Attainable crystallinity at end of draw
12.8	6	6	0
11.1	6	6	0
6.9	8	8	0
4.2	14	14	0
1.8	26	25	5
1.0	52	48	25
0.56	90	50	30
0.24	210	180	70
0.12	425	350	85

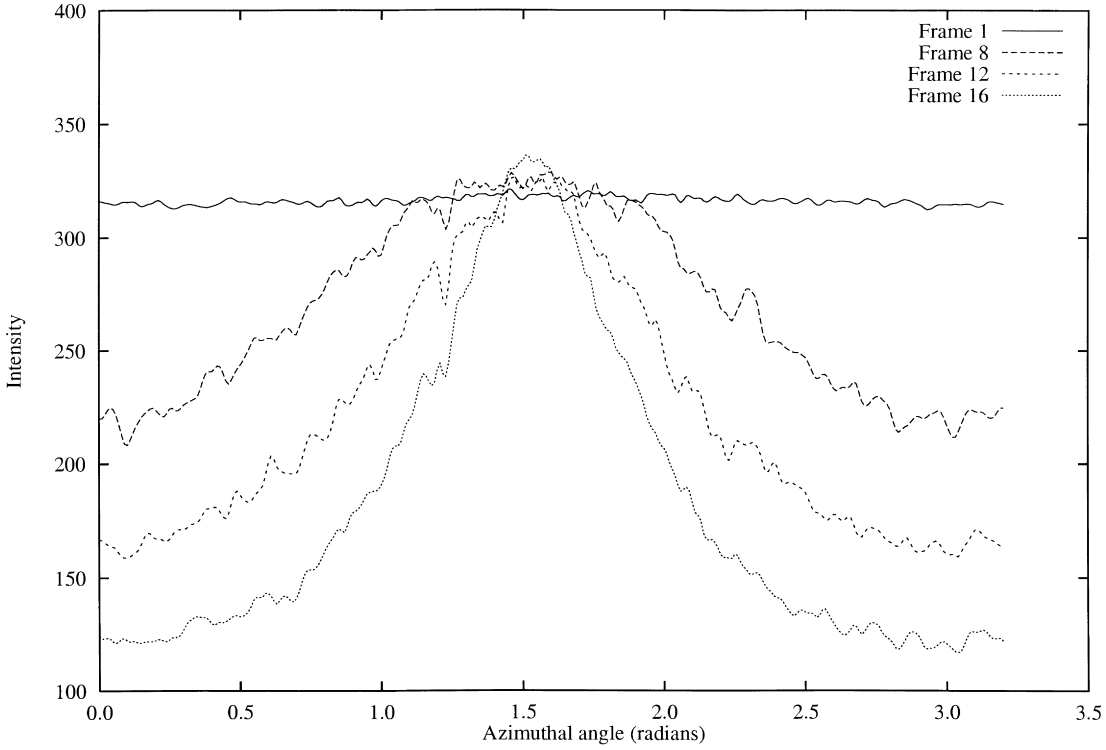

Fig. 5. Series of azimuthal scans at ~0.28 $Å^{-1}$ taken from the diffraction patterns for the sample illustrated in Fig. 1.

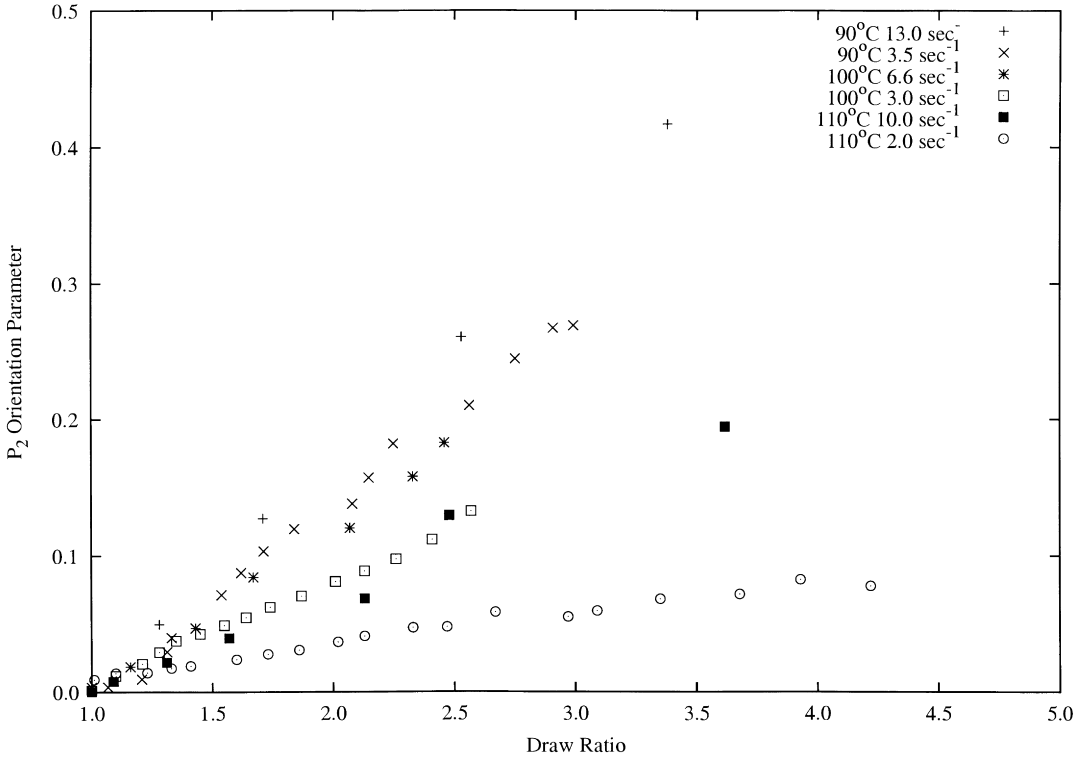

Fig. 6. Plot of draw ratio and the orientation parameter $\langle P_2(\cos\theta)\rangle$ calculated from the X-ray diffraction pattern of PET samples recorded during drawing at 90°C (13.0 s^{-1}, 3.5 s^{-1}), 100°C (6.6 s^{-1}, 3.2 s^{-1}) and 110°C (10.3 s^{-1}, 2.1 s^{-1}).

Table 2
Draw ratio at onset of crystallisation, final draw ratio and crystallisation rates of experiments illustrated in Fig. 6

Draw temperature (°C)	Draw rate (s^{-1})	Draw ratio at onset of crystallisation	Final draw ratio	Crystallisation rate (s^{-1})
90	12.8	3.7	3.7	10.6
90	3.5	3.2	3.2	5.2
100	6.6	2.5	2.9	7.5
100	3.2	2.6	3.5	9.6
110	10.3	3.5	3.8	40.0
110	2.1	4.0	4.7	2.4

combinations of draw rate and temperature. The scatter in the plots reflects the limitation in extracting orientation parameters from the diffuse scattering patterns. The level of orientation achieved for a given draw ratio progressively decreases with increasing temperatures and with decreasing draw rates, indicating a progressive relaxation effect from the entangled chain network competing with the applied deformation.

It will be noted from Fig. 6 that the draw ratio at the end of the deformation phase varies considerably over this set of experiments. This is a manifestation of the variation in degree of necking during the experiments. Some experiments show a more pronounced neck, which enables the deforming section to achieve a higher draw ratio than for a more uniform draw. Table 2 shows in more detail how both final draw ratio and draw ratio at the onset of crystallisation vary in these experiments.

Also shown in Table 2 are the rates of the subsequent crystallisation process. Our previously reported initial experiments noted that crystallisation rate was very dependent on draw ratio and was insensitive to temperature. We also noted that a key feature determining crystallisation was the degree of orientation of the chain segments at the end of the draw process [2]. The data in Table 2 provide evidence that the previous apparent insensitivity to increasing temperature is more likely the result of opposing effects in which enhancement of the rate due to increased segment mobility balances a reduction due to lower segment orientation, partly due to the reduced draw ratio. The dependence of crystallisation rate on drawing conditions will be discussed in more detail in a subsequent paper [20].

4. Discussion

4.1. Oriented networks

The values of $\langle P_2(\cos\theta)\rangle$ achieved for a given draw ratio shown in Fig. 6 are close in magnitude to those found by other workers in which $\langle P_2(\cos\theta)\rangle$ has been measured by well established birefringence methods [10,11]. This agreement validates the above procedure for deriving $\langle P_2(\cos\theta)\rangle$ from azimuthal diffraction scans.

In Fig. 6, the progressive reduction in orientation that is achieved with increasing temperature or reduced draw rate is consistent with chain relaxation competing with the deformation process. At higher temperatures the mobility of the main chain motions enables the oriented chains to retract through the chain entanglements, while at slower draw rates there is increasing opportunity for chains to retract within the same timescale as the deformation. For simplicity, the effectiveness of the deformation in competing with network relaxation can be characterised by the mean slope of $\langle P_2(\cos\theta)\rangle$ vs draw ratio. Fig. 7 shows a plot of the mean slope vs the logarithm of the draw rate based on thirty drawing experiments covering a range of drawing conditions in which temperature, draw rate and final draw ratio were varied. For clarity, the data points for different draw temperatures have been plotted with different symbols. It will be noted that the data points cluster according to temperature into similar, near linear relationships that are shifted relative to the draw rate axis. It is a well established practice in polymer relaxation studies to employ time–temperature superposition methods to unify the effects of temperature and deformation rate. For amorphous polymers in the temperature region above the glass transition it is appropriate to use a WLF relationship for the superposition. Studies by Le Bourvellec have established the following WLF relationship for PET [12].

$$\log_{10} a_T = \log_{10} \frac{\tau_T}{\tau_{84.2}} = -\frac{8.4(T-84.2)}{42.4+T-84.2}$$

where T is temperature in °C.

Fig. 8 shows a modified plot of the same data in which this WLF shift factor has been used to shift the data to a 90°C reference temperature. All the data points now cluster closely around one relationship, which can be regarded as an underlying master curve. The WLF shift demonstrates how temperature and draw rate can be appropriately interchanged to achieve the same overall effects in terms of the response of the chains to deformation of the entangled network.

4.2. Chain relaxation

Current understanding of relaxation of deformed chains is derived from the theoretical framework of Doi and Edwards [16] of an enclosing tube and the concept of reptation introduced by de Gennes [17]. The basic model involves three interlinked mechanisms occurring over different timescale regimes. As a result of macroscopic deformation, the tubes whose topography is defined by entanglements are correspondingly deformed. The fastest relaxation motion, characterised by a relaxation time τ_A, involves the Rouse modes between two entanglements. These motions operate on a time scale in which the entanglements can be considered as fixed and enable the chain strands between the "fixed" entanglements to move to equilibrium configurations. The second relaxation, characterised by τ_B, is enabled by the

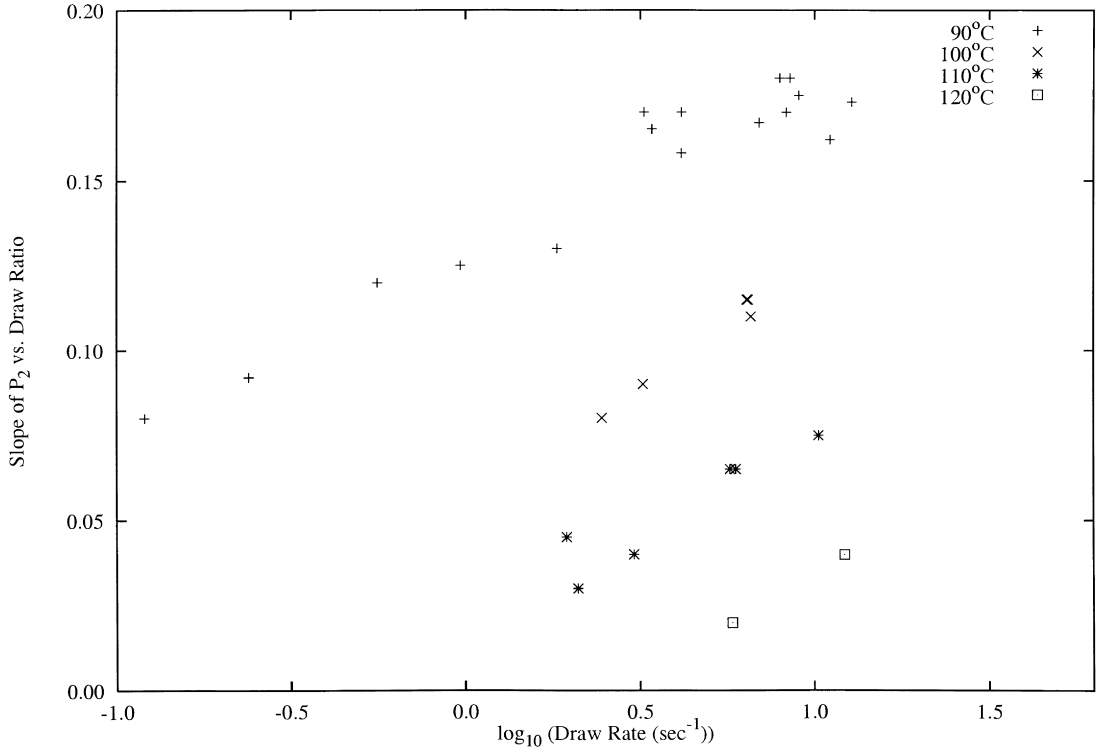

Fig. 7. Variation of slope of plots of $\langle P_2(\cos\theta)\rangle$ vs draw ratio plotted against draw rate for a series of 30 experiments.

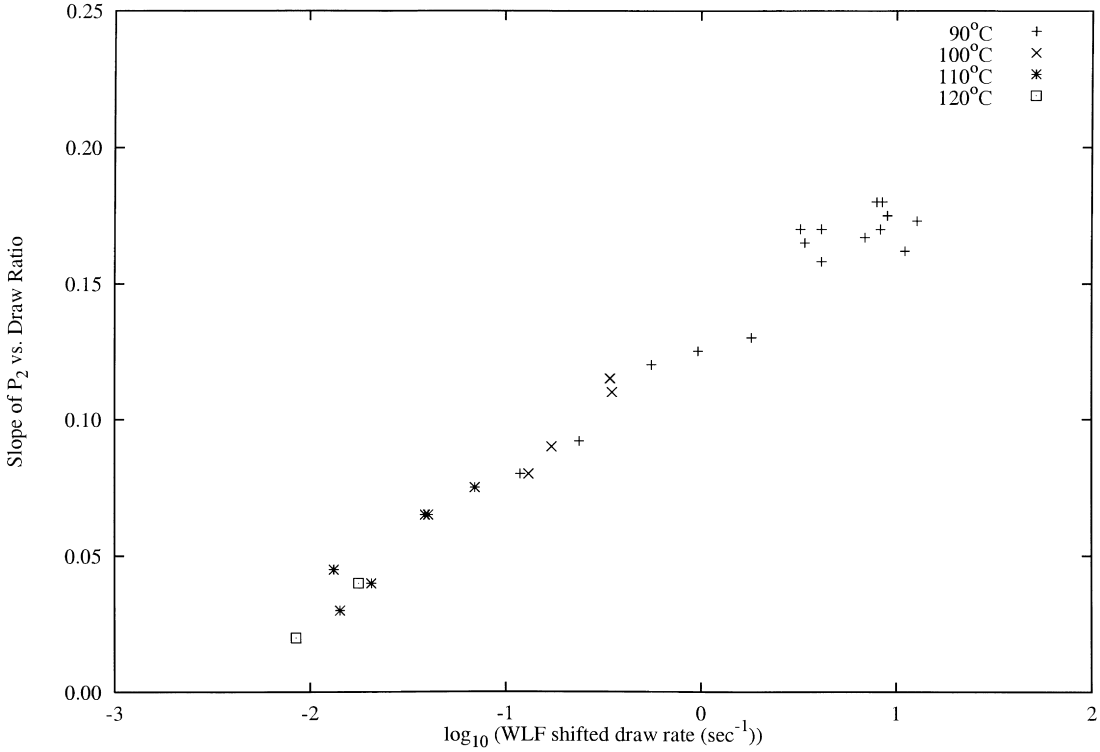

Fig. 8. Variation of slope of plots of $\langle P_2(\cos\theta)\rangle$ vs draw ratio plotted against WLF shifted draw rate for a 90°C reference temperature.

Table 3
Estimates of chain relaxation times assuming $M = 40\,000$; $M_e = 1200$; $\tau_A = 0.001$ s at 90°C

Temperature (°C)	τ_B (s)	τ_C (s)	$1/\tau_B$ (s^{-1})	$1/\tau_C$ (s^{-1})
80	190	19000	0.005	5×10^{-5}
90	2.2	220	0.45	0.0045
100	0.12	12	8.4	0.0833
110	0.015	1.5	66	0.66
120	0.003	0.32	310	3.1
130	0.001	0.10	1000	10

Rouse motions and involves a retraction of chains within the deformed tube in order to recover their equilibrium curvilinear lengths. This process results in a change in the length of strands between entanglements and hence a change in the effective Kuhn lengths N. The third stage, characterised by τ_C, involves the reptation of the chains out of their original deformed tubes to form fresh undeformed tubes and results in the chains attaining isotropic configurations. The fastest motions are related to the molecular weight between entanglements, M_e:

$$\tau_A \sim \frac{\eta}{T} b^2 M_e^2$$

where η is a molecular friction coefficient. The slower relaxations τ_B and τ_C are related to τ_A and the molecular weight M of the polymer through:

$$\tau_B \cong 2\tau_A \left(\frac{M}{M_e}\right)^2$$

$$\tau_C \cong 6\tau_A \left(\frac{M}{M_e}\right)^3.$$

(In view of the polydispersity of PET there is an uncertainty as to the most appropriate values to use for the numerical factors of these scaling relationships [13–15].) Lapersonne [16] has estimated the values of τ_A for PET to be around 10^{-2} s at 85°C and 10^{-4} s at 97°C. The temperature dependence of the Rouse modes is mainly due to the molecular friction coefficient which is expected to be governed by the WLF type of relationship. Table 3 shows estimates of the magnitude of the above three relaxation times based on Lapersonne's data and the WLF shift factors. Also shown in Table 3 are the reciprocals of the relaxation times in order to illustrate the rates of the fundamental mechanisms.

According to these estimates for 90°C, the experimental data in Fig. 8 is spread roughly over the regime of both the retraction and reptation relaxation processes. One can therefore speculate that in the region of the highest draw rate, where the draw rate is faster than the retraction rate, the chain entanglements will act as temporary crosslinks in the time scale of the deformation process. This is the region often referred to as the rubber plateau that occurs at temperatures above but sufficiently close to the T_g. Many workers have demonstrated that in this region, the network can be treated as a simple crosslinked rubber network in which the orientation function can be approximately represented by [17]:

$$\langle P_2(\cos\theta)\rangle = \frac{1}{5N}\left(\lambda^2 - \frac{1}{\lambda}\right).$$

According to this relationship, $\langle P_2(\cos\theta)\rangle$ and λ can be interpreted in terms of the parameter, N, which is the number of Kuhn links in a freely jointed strand of chain between the effective crosslinks. Using our data, the value of N derived in this way varies from around 5 for experiments at 90°C to 20 for the data at 110°C. The lower value is close to estimates from other workers measured on PET drawn at 80°C at slower rates [10,18] and is also consistent with the entanglement molecular weight deduced from rheological data [19]. The experiments with higher values for the effective N indicate that the chain retraction mechanism has been able to operate on the timescales of the deformation process.

4.3. Crystallisation regimes

The relaxation times in Table 3 have implications for the above observations on crystallisation behaviour. It will be noted that the draw rate of $\sim 1\ s^{-1}$, at which there is evidence of crystallisation commencing before the end of the deformation stage, is close to the rate of the chain retraction process. In our previous paper [2] we speculated that the reason that crystallisation does not start until the end of draw is that continuing network deformation frustrates attempts by the chain segments to move into crystallographic register and that only when deformation has stopped can the oriented segments cooperatively align to form crystallographic lattices. The change in behaviour at $\sim 1\ s^{-1}$ is consistent with this and implies that at slower draw rates the chains have the ability to slip through the restraining entanglements in order to move into adjacent register while deformation is still in progress.

Our previous paper also noted that when drawing at rates of $\sim 12\ s^{-1}$ in the temperature range above 125°C, the amorphous diffraction pattern remained essentially isotropic and no oriented crystallisation was observed during the experiments [2]. This is consistent with the reptation rates $1/\tau_C$ in the Table 3 which show that the predicted reptation rate becomes comparable with the draw rate at a temperature of around 130°C. At higher temperatures than this, the chains would be expected to be able to slip out of the deforming tubes faster than the timescale of the drawing process.

In the drawing of PET there are therefore three definable regimes which are closely linked with the fundamental relaxation mechanisms of the entangled chain network. At draw rates faster than $1/\tau_B$, no significant crystallisation is able to commence until after the end of the deformation process. At draw rates slower than $1/\tau_C$, no oriented crystallisation occurs. At intermediate draw rates, oriented

crystallisation can occur but is able to commence during the draw process.

A subsequent paper [20] will deal in more detail with the effect of drawing conditions and relaxation processes on crystallisation rate and crystallite orientation.

5. Conclusions

It has been shown that azimuthal scans of the amorphous halo can give a valid estimate of the $\langle P_2(\cos\theta)\rangle$ orientation parameter during a fast drawing process. An analysis of the influence of drawing conditions on segment orientation has clarified how chain network relaxation processes affect the oriented crystallisation process. It has been demonstrated that the effects of draw rate and temperature can be interrelated by a time–temperature superpostion based on a WLF shift factor. For draw rates faster than the rate of the chain retraction mode, $1/\tau_B$, the onset of crystallisation is delayed until the end of the deformation process. For draw rates slower than the rate of chain reptation, $1/\tau_C$, no oriented crystallisation is observed. For draw rates between the retraction and reptation rates of the network, oriented crystallisation is able to start before the end of the drawing process.

Acknowledgements

We wish to thank Prof. Lucien Monnerie for valuable disussions, particularly on the influence of chain relaxation processes. This work was supported by the allocation of beam time at the ESRF. We are grateful to M. Daniels, M.G. Davies, G. Dudley, E.J.T. Greasley, G. Marsh, M. Wallace and C. Sutton for technical support and help with preparation of the manuscript.

References

[1] Blundell DJ, MacKerron DH, Fuller W, Mahendrasingam A, Martin C, Oldman RJ, Rule RJ, Riekel C. Polymer 1996;37:3303.
[2] Mahendrasingam A, Martin C, Fuller W, Blundell DJ, Oldman RJ, Harvie JL, Mackerron DH, Riekel C, Engstrom P. Polymer 1999;40:5553.
[3] Blundell DJ, Oldman RJ, Fuller W, Mahendrasingam A, Martin C, MacKerron DH, Harvie JLRJ, Riekel C. Polym Bull 1999;42:357.
[4] Salem DR. Polymer 1992;33:3182.
[5] Le Bourvellec G, Monnerie L. Polymer 1986;27:856.
[6] Middleton A, Duckett RA, Ward IM, Mahendrasingam A, Martin C. In preparation.
[7] Biangardi HJ. J Polym Sci, Polym Phys Edn 1980;18:903.
[8] Blundell DJ, Chivers RA, Curson AD, Love JC, MacDonald WA. Polymer 1988;29:1459.
[9] Lovell R, Mitchell GR. Acta Cryst A 1981;37:135.
[10] Cunningham A, Ward IM, Willis HA, Zichy V. Polymer 1974;15:749.
[11] Perena JM, Duckett RA, Ward IM. J Appl Polym Sci 1980;25:1381.
[12] Le Bourvellec G. Thesis Doct Ing, Universite Pierre et Marie Curie, Paris, 1984.
[13] Doi M, Edwards SF. The theory of polymer dynamics. Oxford: Clarendon Press, 1986.
[14] de Gennes P-G. J Chem Phys 1971;55:572.
[15] Viovy JL, Monnerie L, Tassin JF. J Polym Sci (Polym Phys) 1983;21:2427.
[16] Lapersonne. PhD, Thesis, Universite Pierre et Marie Curie, Paris, 1991.
[17] Roe RJ, Krigbaum WR. J Appl Phys 1964;35:2215.
[18] Nobbs JH, Bower DI, Ward IM. Polymer 1976;17:25.
[19] Fetters LJ, Lohse DJ, Richter D, Witten TA, Zirkel A. Macromolecules 1994;27:4639.
[20] Mahendrasingam A, Blundell DJ, Martin C, Fuller W, MacKerron DH, Harvie JL, Oldman RJ, Riekel C. Polymer 2000;41:7803.